Fire Technology

https://doi.org/10.1007/s10694-020-01036-3

# Bayesian Inference of Fire Evolution Within a Compartment Using Heat Flux Measurements

*Jan-Michael Cabrera* * *and Ofodike A. Ezekoye, Department of Mechanical Engineering, The University of Texas at Austin, Austin, TX 78712, USA*
*Robert D. Moser, Institute for Computational Engineering and Sciences, The University of Texas at Austin, Austin, TX 78712, USA*

**Received:** 5 June 2020/**Accepted:** 20 August 2020

***Abstract.*** The dynamical evolution of a multiple fuel package fire leaves thermal signatures. For practical and theoretical reasons, it is important to determine conditions in which one can identify the path the system took by conducting a set of experiments that cover the space of all possible paths. An experimental fire compartment capable of producing repeatable and highly customizable fire-evolution scenarios is presented. Instrumented propane burners are configured in the compartment each with a simple critical heat flux ignition model. Heat flux sensors are located around the burner configuration to provide temporal incident heat flux measurements. Data from several hypotheses representing possible scenarios are compared to data generated using some *true* configuration using a Bayesian methodology. The Bayesian methodology is able to illicit the correct fire-evolution scenario from the set of hypotheses with a high degree of confidence. The information content provided by each sensor is analyzed to highlight the importance of sensor location in determining the fire-evolution. Posteriors for the hypotheses using two different error structures are also compared over the sensors to highlight the importance of choosing the correct error structure.

**Keywords:** Fire forensics, Bayesian statistics, Inverse problems, Compartment experiments, Fire experiments

## 1. Introduction

*NFPA 921, Guide for Fire and Explosion Investigations* provides guidance for a fire investigator to create and test hypotheses in a disciplined manner in an attempt to reduce biases and standardize the investigation process [1]. Inevitably, because of the destructive nature of the fire dynamical processes within a compartment, there will be uncertainty associated with the details of the fire scene. Evidence at the fire scene allows a fire investigator to form hypotheses corresponding to the pre-fire layout, fuel load, ventilation conditions, etc. Further evidence from the scene in

* Correspondence should be addressed to: Jan-Michael Cabrera, E-mail: janmichael.cabrera@gmail.com

Published online: 18 September 2020

the form of fire patterns, damage to objects, witness statements, etc., are then used by the investigator in an attempt to narrow down the hypothesis space. This process may also sometimes bring to light hypotheses not previously taken into consideration at the start of an investigation. Often times testing of particular hypotheses are conducted in an attempt to recreate the evidence found at the fire scene. This investigation process is performed, sometimes multiple times, until a single hypothesis that best matches the fire scene evidence remains, or the cause/origin of the fire is declared undetermined. A fire is usually undetermined when there is too much uncertainty in the evidence available and narrowing down the hypothesis space is not possible, or more than a single hypothesis is consistent with the collected evidence.

Despite the principled manner in which fire investigation should take place, there was little guidance on how an investigator might statistically weight the evidence gathered and little guidance to making quantitative inferences of the possible hypotheses. This is highlighted by the fact that the U.S. National Academies has reported shortcomings in the application of forensic science used in prosecution in recent years [2]. Recent research, therefore, aims to address these shortcomings with origin determination being a critical factor. Without origin determination NFPA 921 suggests cause cannot be determined. Gorbett and Chapdelaine arrange the sub-processes of origin determination outlined in NFPA 921 in a manner that is more consistent with the scientific method to aid the fire investigator in forming and testing of fire scene hypotheses [3]. Gorbett et al. also discuss the origin matrix method, a tool developed by Cox [4] to help an investigator narrow down an area of origin, but note that the methodology needs systematic evaluation [5]. The application of a methodology, specifically the process of origin determination (POD), was shown to increase the accuracy of origin determination of a sample of participants compared to those not informed of the methodology [6]. The participants were tasked with narrowing down the area of origin based on synthetic normalized integrated heat flux measurement contours produced by fires of differing sizes, peak times, and locations simulated in Fire Dynamics Simulator (FDS) and visualized in Smokeview. Gorbett et al. also report that using fire patterns remains at the core of identifying fire origin within a compartment with most investigators opting to not make damage measurements in the compartment and instead relying on visible damage signatures [5]. Hopkins et al. showed that initial fire patterns from a fire plume can persist post-flashover, however the tests were dominated by single heat sources and reported large variability in the observed fire patterns [7]. Madrzykowski and Fleischmann aimed to characterize pre-flashover fire patterns and the associated uncertainties noting that uncertainties in fire patterns increased with increasing fuel complexity [8]. In a direct response to the National Academy of Sciences statement, UL Fire Safety Research Institute present and make publicly available data from a large suite of tests on single family homes to assess the impact of ventilation conditions on fire damage and patterns [9].

While there continues to be excellent work being conducted by the fire community in researching new predictive models and analyzing novel ignition scenarios (e.g. lithium-ion batteries, see Stauffer for a comprehensive review over the past

few years [10]), most compartment scale experiments are being conducted with either single fires, or single scenarios, usually with fuel packages that produce variable heat release rate (HRR) curves. An area of research that is in need of further development is the quantification of the plausibility of various scenarios given the uncertainty in measured quantities of interest. Bayesian inference provides the framework to accomplish just this; it seeks to quantify degrees of beliefs for hypotheses given observed evidence and its associated uncertainty. Recently, Nordgaard and Rasmusson highlight the importance of the Bayesian approach when deriving likelihood ratios in the context of the forensic sciences [11].

Bayesian methods have been making a resurgence in many fields and have been applied successfully to a number of fire problems [12–14]. Overholt and Ezekoye, for example, applied these techniques to infer the HRR for temporal temperature measurements in simulated room-scale experiments, and to determine the size or location of a fire of constant HRR within a compartment [15–17]. Kurzawski et al. also exercised an inversion framework aimed at simultaneous localization and HRR characterization of a fire within a compartment given time-integrated heat flux data throughout the compartment with two separate forward models [18]. This paper focuses on the quantification of hypotheses that represent different fire evolution scenarios. An instrumented experimental compartment capable of combining user-defined HRRs and secondary ignition criteria for producing repeatable and customizable multi-burner/multi-hypothesis fire evolution scenarios is described in Sect. 4. The location of combustible items in the compartment is known and what is not known is which of the combustible items originated the fire evolution in the compartment. The setup is utilized to generate *true* temporal incident heat flux measurements, measured using directional flame thermometers (DFTs), at various locations in the compartment. In place of witness information, fire patterns, etc., the setup is also utilized to collect temporal heat flux measurements from plausible fire-evolution hypotheses presented in Sect. 4. A Bayesian framework, introduced in Sect. 3, is then applied on the observed quantities for quantifying the probability of the different scenarios, taking into account the uncertainties in measurement data presented in Sect. 4. The effect of different error models of the data on the probability of the different scenarios is also investigated.

## 2. Experimental Facility

An experimental compartment previously utilized for various room scale fire experiments including positive pressure ventilation [19], wildfire fuel bed characterization [20], and HRR inversion [21] at the J.J. Pickle Research Campus at the University of Texas at Austin was used to conduct compartment scale multiple hypothesis tests. Two sand burners 0.3 m by 0.3 m square by 0.3 m tall constructed in accordance with the *NFPA 286* and one 0.3 m by 0.3 m square by 0.15 m tall gas burner were each electronically controlled using PID mass flow controllers to follow specified HRRs upon reaching some ignition criteria [22]. Each burner was instrumented with four modified DFTs with centers 0.2 m above

the ground to measure the incident heat flux. Eight modified DFTs were also placed around the three burner setup all 0.7 m above the ground to measure incident heat flux. The modified DFTs are constructed similarly to standard DFTs (see ASTM E3057 [23]) but with a smaller form factor. Construction and calibration of the modified DFTs are discussed in [24].

Compartment geometry, burner and sensor locations, and burner/sensor coordinates are shown in Fig. 1 and a typical fire evolution experiment is shown in Fig. 2. Setpoint signals sent to the mass flow controllers and data acquisition rates for the DFTs were set to 1 Hz for all experiments. A simple critical heat flux secondary ignition model was chosen for its simplicity to reduce the computational burden of the control and data acquisition system. A typical test consisted of initializing a single burner in the compartment and allowing it to follow a specified HRR. Throughout the test the adjacent burners would sense incident heat fluxes until the ignition criteria was met. When a burner reached the ignition criteria, it would follow its own HRR ramp. Scoping tests were completed to test the limits of the three burner setup and the commercially sourced propane supply. The scoping tests showed that the fuel supply could only sustain a maximum total HRR of roughly 250 kW due to the tank size utilized and ambient temperature conditions. A 100 kW peak triangle fire was determined to be the maximum size fire any one burner could sustain to satisfy this constraint. Scoping tests also showed that the critical heat flux for ignition needed to be below 8 $kW/m^2$ for adjacent burners to ignite given a 100 kW peak triangle fire for the initial burner. During the scoping tests, the development of a hot gas layer (HGL) was observed, but did not contribute to the heat flux response of the DFTs.

A total of four fire-evolution tests were conducted each with duration 720 s. For all four tests, the burners in the compartment followed a triangular HRR ramp as shown in Fig. 3 once the ignition criteria for a particular burner was met. The first test conducted began with the first burner (B1) beginning its HRR ramp at 0 s. Burners 2 and 3 were set to initiate their respective HRR ramps when any one of the four DFTs on the burners measured an incident heat flux greater than 5 $kW/m^2$. Spacing between burners varied to ensure burners activated sequentially. This test was used to generate the ''true'' incident heat flux measurements at the eight DFTs in the compartment. The heat flux measurements in subsequent tests would be compared to the ''true'' values to test ignition sequence hypotheses. Three more tests were conducted corresponding to the three possible hypotheses: (1) the first burner began the fire evolution, (2) the second burner began the fire evolution, and (3) the third burner began the fire evolution. The scenarios presented represent a simple set in which the HRR of the involved items, the compartment layout, and the ignition criteria are perfectly known; the only unknown is which scenario produced the observed data. Sect. 3 outlines application of the Bayesian framework to this fire evolution problem.

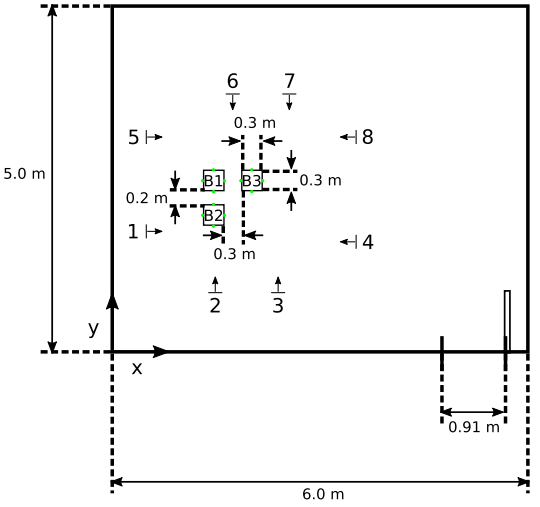


(a)

| Object | x (m) | y (m) |
|---|---|---|
| B1 | 1.50 | 2.60 |
| B2 | 1.50 | 2.00 |
| B3 | 2.20 | 2.60 |
| S1 | 0.50 | 1.65 |
| S2 | 1.40 | 0.86 |
| S3 | 2.30 | 0.86 |
| S4 | 3.30 | 1.50 |
| S5 | 0.50 | 3.00 |
| S6 | 1.65 | 3.70 |
| S7 | 2.46 | 3.70 |
| S8 | 3.30 | 3.00 |

(b)

**Figure 1. (a) Experimental compartment layout for the four forward cases. The burners were standard 0.3 m by 0.3 m square sand burners each instrumented with a modified DFT on each side to measure incident heat flux. Burner centroids and sensor locations are shown in (b). Arrows on sensors indicate sensing direction. All eight sensors were installed 0.7 m above the ground.**

**Figure 2. Photo of three burner fire evolution test captured through open door in the compartment during scoping tests. The HRR of burners 1, 2, and 3 were at roughly 70 kW, 100 kW, and 50 kW respectively. Flame heights remained well below the ceiling and minimal flame leaning was observed.**

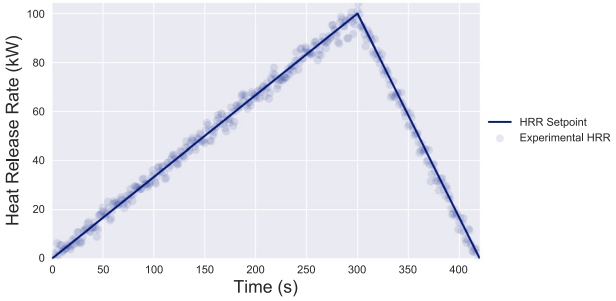


**Figure 3. HRR setpoint and representative experimental HRR curve used for each of the three burners for the four tests conducted. The HRR ramps up from 0 kW to 100 kW in 300 s and then ramps back down to 0 kW at 420 s. The HRR of the burner begins after the ignition criteria for a burner is met. All times are shifted depending on burner activation time.**

## 3. Bayesian Framework

A hypothesis is tested by conducting an experiment that produces data and comparing those data to the archived true data. This process can be cast as an optimization problem that can be solved multiple ways. For example one could use a maximum likelihood method which requires the definition of a likelihood across hypotheses and subsequently choosing the scenario that produces the largest likelihood:

$$\hat{H} = \arg\max_{H_i \in \mathbf{H}} \{P(D|H_i)\}, \tag{1}$$

where $\mathbf{H}$ is the set of possible scenarios that may have generated the data, $D$. While the maximum likelihood method allows one to rank the hypotheses, a downside for determining which hypothesis is true is that it is difficult to quantify by how much one hypothesis is more true than another. Yet another difficulty is that the maximum likelihood method does not take into account the uncertainty associated with the observed measurements. For these reasons the Bayesian framework is applied for assigning probabilities to each hypothesis. Section 3.1 outlines the application of Bayes' Rule to inference on fire evolution scenarios and Sect. 3.2 illustrates how one might make estimates of the correlated errors in heat flux measurements for quantifying the total uncertainty.

### 3.1. Bayesian Inference for Fire Evolution

Bayes' Rule applied to the discrete hypothesis space of interest is,

$$P(H_i|D) = \frac{P(H_i)P(D|H_i)}{\sum_{i'=1}^{I} P(H_{i'})P(D|H_{i'})}, \tag{2}$$

where $P(H_i|D)$, the posterior probability of a hypothesis, represents the probability of a scenario after having observed the data, $D$. $P(H_i)$ is known as the prior probability for a particular hypothesis and represents a discrete distribution over possible scenarios. The prior represents one's state of knowledge before observing the data and is often times assigned a uniform distribution to represent a state of ignorance (one should only favor a hypothesis over another if there is evidence to support this). $P(D|H_i)$ is the likelihood function and it is not a proper probability distribution. It quantifies the comparison between the data collected and the data generated by a particular scenario. The term in the denominator, $\sum_{i'=1}^{I} P(H_l)P(D|H_l)$, is known as the Bayesian evidence or the marginal likelihood and is often ignored as it acts as a normalizing constant to ensure that the posterior is a proper probability distribution (i.e. $\sum_{i=1}^{I} P(H_i|D) = 1$).

Defining the likelihood requires establishing a statistical model that makes assumptions about the errors present. The statistical model chosen is,

$$q_j = \hat{q}_{ij} + e_j;\ e_j \sim N(0, \Sigma_j);\ \Sigma_j = \hat{\Sigma}_j + \sigma^2 I, \tag{3}$$

where $q_j$ is a vector of measured incident heat fluxes (these can be smoothed or the raw signal) of length $N$ representing the true configuration at each $j$ sensor in the compartment, $\hat{q}_{ij}$ is a vector of measured incident heat fluxes for each hypothesis $i$ and sensor $j$, and $e_j$ represents the error structure of a particular sensor. Here it is assumed that the errors are temporally correlated and that the correlation structure can be parameterized by a multivariate normal distribution with zero mean and covariance, $\Sigma_j$. It is further assumed that the correlated errors arise from two sources: (1) temporally correlated errors due to the temporally correlated process that generates the incident heat fluxes, $\hat{\Sigma}_j$, and (2) independent and identically distributed (iid) errors associated with uncertainty in the true value of the measured incident heat fluxes (a standard deviation of roughly 1 kW/m$^2$ for the DFTs). If the temporal correlations of the incident heat flux measurements are not taken into consideration, the confidence in a particular hypothesis will be overestimated. The likelihood for a single sensor is then,

$$P(\hat{q}_{ij}|q_j, \Sigma_j, H_i) = \frac{1}{(2\pi)^{N/2}|\Sigma_j|^{1/2}} \exp\left(-\frac{1}{2}(\hat{q}_{ij} - q_j)^T \Sigma_j^{-1} (\hat{q}_{ij} - q_j)\right). \tag{4}$$

To simplify the analysis, the sensors are assumed to have minimal spatial correlation. The full likelihood is then,

$$P(D|H_i) = \prod_{j=1}^{J} P(\hat{q}_{ij}|q_j, \Sigma_j, H_i). \tag{5}$$

Substituting Eq. 5 into Eq. 2 and letting $P(H_i) = h_i$, the posterior becomes,

$$P(H_i|D) = \frac{h_i \cdot \exp\left[-\frac{1}{2}\sum_{j=1}^{J}(\hat{q}_{ij} - q_j)^T \Sigma_j^{-1}(\hat{q}_{ij} - q_j)\right]}{\sum_{i'=1}^{I} h_{i'} \cdot \exp\left[-\frac{1}{2}\sum_{j=1}^{J}(\hat{q}_{i'j} - q_j)^T \Sigma_j^{-1}(\hat{q}_{i'j} - q_j)\right]}. \tag{6}$$

While Eq. 6 is a closed form expression for the posterior, an estimate of the correlated errors, $\hat{\Sigma}_j$, still needs to be defined. The following section, Sect. 3.2, illustrates the estimation of this parameter.

### 3.2. Uncertainty Quantification

In general, uncertainty is composed of two parts: aleatoric uncertainty and epistemic uncertainty. Aleatoric uncertainty pertains to uncertainty associated with random, noise generating process (e.g. electronic noise) and epistemic uncertainty relates to the knowledge available (e.g. predictions by a model or certainty in a calibration parameter). The errors associated with the incident heat flux measurements are a combination of both aleatoric and epistemic uncertainties pertaining to the calibration process of the data reduction model for the DFTs on noisy temperature measurements [24]. There is another source of aleatoric uncertainty associated with the fire-evolution problem. The act of performing a test in the manner presented in Sect. 2 requires that a possibly noisy electronic signal be sent to a mass flow controller, which is in turn interpreted by the controller itself with some internal model to match pressure measurements over a laminar flow element to the temporally changing setpoint. These uncertainties are translated to uncertainties in the HRR of a particular burner. Atmospheric conditions in the test setup as well as other factors also add noise to the signals measured by the incident heat flux measurements in the compartment, both on the burners and the sensors placed throughout. The result is that there will be uncertainty in the ignition events for nominally similar configurations which will ultimately lead to temporally correlated uncertainty in the incident heat flux measurements.

To model the temporally correlated errors in the incident heat flux measurements, a similar statistical model to that presented in Sect. 3.1 is proposed,

$$\hat{q}_{jk} = \bar{q}_j + \hat{e}_j;\ \hat{e}_j \sim N(0, \hat{\Sigma}_j). \tag{7}$$

Here, $\bar{q}_j$ represents the incident heat flux one would measure if no noise were present in the mass flow controller, environment, etc. at sensor $j$, and $\hat{q}_{jk}$ is the vector of measured incident heat fluxes for replicate $k$ of an experiment. The culmination of errors present in the experimental setup is characterized by a mean zero multivariate normal distribution with covariance $\hat{\Sigma}_j$. Explicitly for a single experiment this is,

$$P(\bar{q}_j|\hat{q}_{jk},\hat{\Sigma}_j)=\frac{1}{(2\pi)^{n/2}|\hat{\Sigma}_j|^{1/2}}\exp\left(-\frac{1}{2}(\hat{q}_{jk}-\bar{q}_j)^T\hat{\Sigma}_j^{-1}(\hat{q}_{jk}-\bar{q}_j)\right). \tag{8}$$

The likelihood for $K$ experiment replicates assuming the replicates are iid is then,

$$P(D|\bar{q}_j,\hat{\Sigma}_j)=\prod_{k=1}^{K}P(\bar{q}_j|\hat{q}_{jk},\hat{\Sigma}_j). \tag{9}$$

One need only find $\bar{q}_j$ and $\hat{\Sigma}_j$ to characterize the errors associated with Eq. 7 because the multivariate normal distribution is uniquely characterized by its mean and covariance. Here a maximum likelihood method is used to estimate $\bar{q}_j$ and $\hat{\Sigma}_j$ from $K$ experiments resulting in,

$$\hat{\Sigma}_j=\frac{1}{K}\sum_{k=1}^{K}(\hat{q}_{jk}-\bar{q}_j)(\hat{q}_{jk}-\bar{q}_j)^T;\bar{q}_j=\frac{1}{K}\sum_{k=1}^{K}\hat{q}_{jk}. \tag{10}$$

In Sect. 4 analysis of the recorded data from the experiments discussed in Sect. 2 using the methodology outlined in this section is discussed.

## 4. Experimental Results

Ignition times of the burners for the four compartment scale experiments outlined in Sect. 2 are presented in Table 1, and the temporally smoothed incident heat flux responses for each of the eight sensors of the *truth*, *hypothesis one*, *hypothesis two*, and *hypothesis three* are shown in Fig. 4 in blue, orange, green, and red bold lines respectively. The raw responses recorded by the DFTs are shown in the same color with low alpha values (i.e. increased transparency). The smoothed curves are shown to highlight the differences (and similarities) in incident heat flux measurements across the tests.

Smoothing of the raw DFT heat flux measurements was performed using Gaussian Process Regression (GPR). GPR is a Bayesian method for characterizing a non-parametric function in terms of a multivariate normal distribution. A maximum-marginal log-likelihood method was used to determine the hyper-parameters of the GP for each vector of measured heat fluxes which is standard practice in the GPR literature. For more details a full description of the GPR methodology can be found in Rasmussen and Williams [25].

The similarities in incident heat flux response between the *truth* and *hypothesis one* should be immediately apparent considering they represent the same experimental configuration. Interestingly there are sensors in the compartment that show similar heat flux measurements across all tests, notably sensors three and four. All other sensors in the compartment show significant differences. The ramifications of this are analyzed later in this section.

Visually, one could at this point determine that *hypothesis one* corresponds to the true configuration using data recorded from all eight sensors. However, if one

**Table 1**
**Burner Ignition Times Across the Different Fire Evolution Scenarios**

| – | Burner 1 (s) | Burner 2 (s) | Burner 3 (s) |
|---|---|---|---|
| Truth | 0 | 119 | 252 |
| Hypothesis 1 | 0 | 113 | 220 |
| Hypothesis 2 | 125 | 0 | 298 |
| Hypothesis 3 | 159 | 273 | 0 |

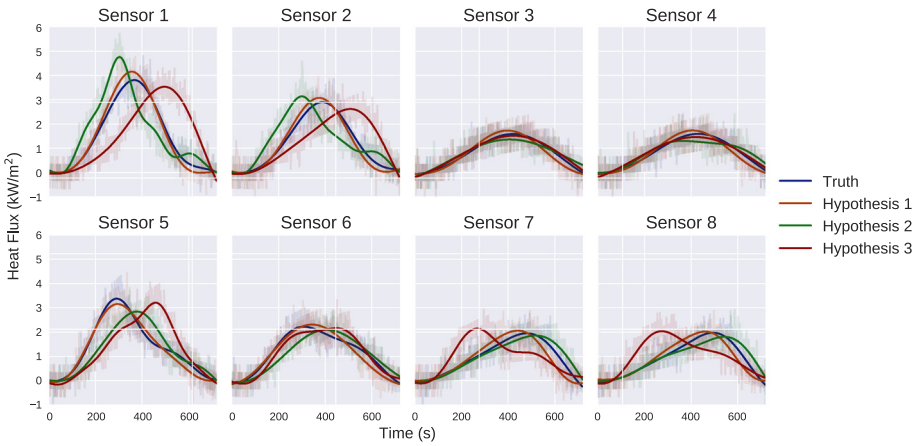


**Figure 4. Incident heat fluxes at each sensor for each of the four tested scenarios: *truth* (blue), *hypothesis one* (orange), *hypothesis two* (green), and *hypothesis three* (red). The raw incident heat fluxes are plotted with low alpha and the smoothed incident heat fluxes are superimposed over the raw values to help illustrate the differences in measured fluxes between scenarios (Color figure online).**

were to use measurements from only a single sensor, say sensor three, one would be hard pressed to determine the true scenario visually. To make a quantitative assessment, however, of the possible scenarios, $\bar{q}_j$ and $\hat{\Sigma}_j$ for each sensor are found using Eq. 10 along with data from the true configuration and *hypothesis one*. It is possible that the actual processes vary from the mean, $\bar{q}_j$, more or less than what is characterized by $\hat{\Sigma}_j$ from only two tests. Given a larger number of resources it would be beneficial to perform more tests of each configuration to obtain better estimates of $\bar{q}_j$ and $\hat{\Sigma}_j$.

Figure 5 shows the smoothed incident heat flux at each sensor for the *truth* and *hypothesis one* in blue and orange respectively. One-hundred samples from a multivariate normal distribution parameterized by $\bar{q}_j$ and $\hat{\Sigma}_j$ are also shown for each sensor in black with low alpha. The plots show that from the information available from the two tests, estimates of the correlated errors were able to be found.

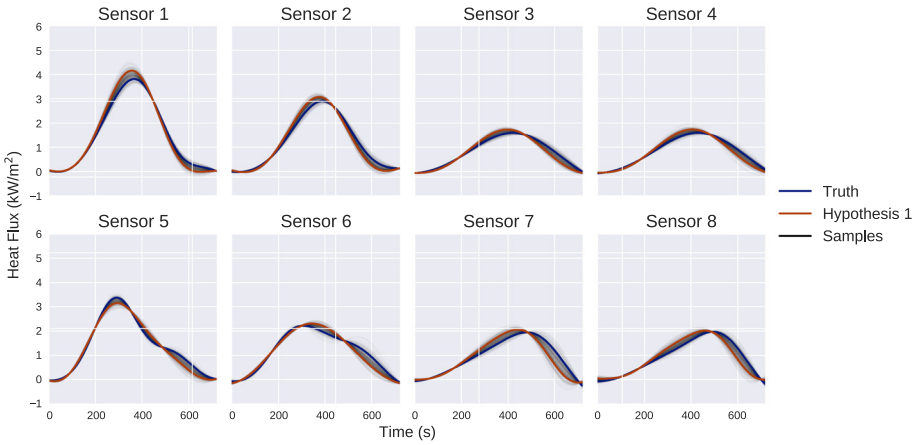


**Figure 5. Smoothed incident heat fluxes at each sensor for replicate tests: *truth* (blue) and *hypothesis one* (orange). The black lines represent 100 samples drawn from a multivariate normal with mean and covariance described by Eq. 10 for each sensor (Color figure online).**

A uniform prior was used (i.e. $h_i = 1/3$) and with the $\hat{\Sigma}_j$s characterized, posterior values for each hypothesis could be calculated using Eq. 6. Using all eight sensors, the posterior probability for each hypothesis for both smoothed and unsmoothed incident heat flux measurements are presented in Table 2. Unsurprisingly, the data available were informative enough that the true configuration, *hypothesis one*, was determined correctly with a high degree of confidence.

Of interest is the information provided by each individual sensor alone. The Kullback-Leibler divergence or relative entropy is able to provide a measure for the distance between two probability distributions. Applied in a Bayesian setting the KL divergence allows one to quantify the amount of learning one can achieve from the data (i.e. the distance between the prior distribution and the posterior). The KL divergence applied to the problem at hand for an individual sensor is defined as,

$$D_{\mathrm{KL}}(P(\mathbf{H}|x_j)||P(\mathbf{H})) = \sum_{i=1}^{I} P(H_i|x_j)\log\left(\frac{\mathrm{P(H_i|x_j)}}{\mathrm{P(H_i)}}\right) \tag{11}$$

where $P(H_i|x_j)$ is the posterior for scenario $H_i$ calculated using only a single sensor:

$$P(H_i|x_j) = \frac{h_i \cdot \exp\left[-\frac{1}{2}(\hat{q}_{ij} - q_j)^T \Sigma_j^{-1}(\hat{q}_{ij} - q_j)\right]}{\sum_{i'=1}^{I} h_{i'} \cdot \exp\left[-\frac{1}{2}(\hat{q}_{i'j} - q_j)^T \Sigma_j^{-1}(\hat{q}_{i'j} - q_j)\right]}. \tag{12}$$

**Table 2**
**Posteriors for Each Hypothesis for Smoothed and Unsmoothed Heat Fluxes**

| – | $P(H_1\|D)$ | $P(H_2\|D)$ | $P(H_3\|D)$ |
|---|---|---|---|
| Smoothed Fluxes | 1 | 0 | 0 |
| Unsmoothed Fluxes | 1 | 0 | 0 |

The units of the KL divergence are in *nats* if the natural logarithm is used or in *bits* if the base of the logarithm is two. The KL divergence was calculated for each sensor for both smoothed and unsmoothed incident heat fluxes with values shown in bits (see Table 3).

As was shown in Fig. 4, sensors three and four showed very similar heat flux responses across all experimental test runs. This is reflected in the KL divergence measure of 0.572 bits and 1.120 bits for sensors three and four respectively for the smoothed heat fluxes. Note that the maximum information gain available from a uniform prior to full confidence in a prediction is 1.585 bits. Similarly the heat flux response of sensors seven and eight are visually similar for hypotheses one and two resulting in KL divergence measures less than 1.585 bits. However, because the heat flux measurements for sensors seven and eight from hypothesis three differed from the other two hypotheses, the KL divergences for these sensors were still greater than the KL divergence measures of sensors three and four. Using the unsmoothed heat fluxes, the KL divergence for all sensors is at this maximum value. The discrepancy between the smoothed and unsmoothed KL divergences are likely due to the fact that some temporal information is lost in the smoothing process of the raw incident heat flux signal.

The effect of the similarities in sensor measurements for sensors three and four can also be seen in the posterior distribution for these sensors. Figure 6 shows the posterior distribution over the hypotheses calculated for each sensor using Eq. 12. Sensors three, four, and even seven show lower confidence in the true configuration with sensor three showing similar posterior values for *hypothesis one* and *hypothesis three*. This is a scenario in which if only sensor three were used to determine the fire-evolution, the origin of the fire might be considered undetermined.

To illustrate the importance of including the correlated aspect of the temporal heat flux measurements, posteriors for each hypothesis were calculated assuming that all heat flux measurements were independent. The likelihood for a single sensor is,

$$P(x_j|H_i) = \left(\frac{1}{2\pi\sigma^2}\right)^{N/2} \exp\left(-\frac{1}{2\sigma^2}\sum_{n=1}^{N}(\hat{q}_{ijn} - \bar{q}_{jn})^2\right), \tag{13}$$

**Table 3**
**KL Divergence Calculated for Each Sensor for the Smoothed and Unsmoothed Incident Heat Fluxes**

| | $D_{\mathrm{KL}}(P(\mathbf{H}\|x_j)\|\|P(\mathbf{H}))$ | |
|---|---|---|
| Sensor No. | Smoothed | Unsmoothed |
| Sensor 1 | 1.585 | 1.585 |
| Sensor 2 | 1.585 | 1.585 |
| Sensor 3 | 0.572 | 1.585 |
| Sensor 4 | 1.120 | 1.585 |
| Sensor 5 | 1.585 | 1.585 |
| Sensor 6 | 1.585 | 1.585 |
| Sensor 7 | 1.422 | 1.585 |
| Sensor 8 | 1.584 | 1.585 |

Sensors with higher $D_{KL}$ provide more information for differentiating hypotheses than sensors with lower $D_{KL}$. The units of $D_{KL}$ are in bits

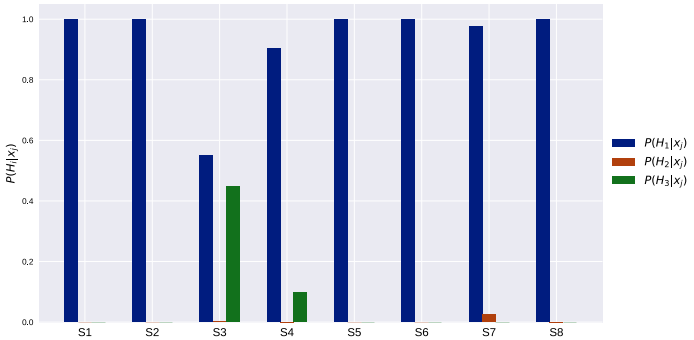


**Figure 6. Posterior distribution calculated using the smoothed response of a single sensor. This was completed for each sensor. Blue, orange, and green bars correspond to posteriors for *hypothesis one*, *hypothesis two*, and *hypothesis three* respectively (Color figure online).**

resulting in the posterior for a given hypothesis:

$$P(H_i|x_j) = \frac{h_i \cdot \exp\left[-\frac{1}{2\sigma^2}\sum_{n=1}^{N}(\hat{q}_{ijn} - \bar{q}_{jn})^2\right]}{\sum_{i'=1}^{I} h_{i'} \cdot \exp\left[-\frac{1}{2\sigma^2}\sum_{n=1}^{N}(\hat{q}_{i'jn} - \bar{q}_{jn})^2\right]}. \tag{14}$$

Figure 7 shows the posterior distribution for the hypotheses calculated for each sensor using Eq. 14. For the sensors whose incident heat fluxes were substantially

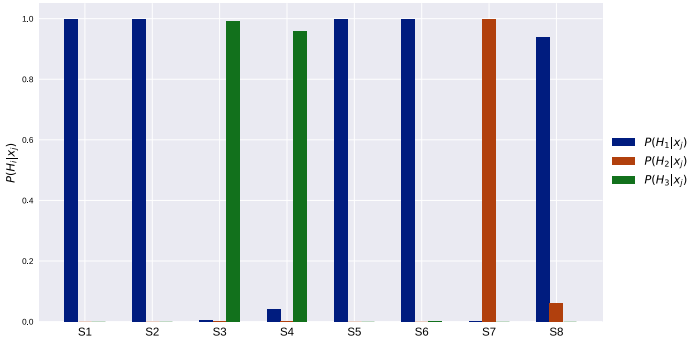


**Figure 7. Posterior distribution calculated using the smoothed response of a single sensor assuming no temporal correlation in the heat flux measurements. This was completed for each sensor. Blue, orange, and green bars correspond to posteriors for *hypothesis one*, *hypothesis two*, and *hypothesis three* respectively (Color figure online).**

different across scenarios, the sensor is able to distinguish the correct hypothesis with a high degree of accuracy. Sensors three, four, and seven, however, predict the incorrect hypothesis with a high degree of confidence. This highlights the need to incorporate the temporal correlations in the measured signal. Not including the temporal correlations can result in over confident predictions.

A more traditional uncertainty analysis of the eight sensors was also conducted to compare against the Bayesian methods presented. The total expanded uncertainty of a heat flux measurement was defined as,

$$\bar{q}_{jn} \pm t^{*}\sigma \tag{15}$$

where $t^{*}$ is 1.96 for a confidence level of 95% assuming the data are normally distributed for sensor $j$ at time point $n$. Heat flux data recorded from the three hypotheses are tested to check if they fall within the interval,

$$\bar{q}_{jn} - t^{*}\sigma \leq \hat{q}_{ijn} \leq \bar{q}_{jn} + t^{*}\sigma. \tag{16}$$

The percentage of points that fall within the interval was calculated for each hypothesis and presented in Table 4. Because of the relatively large uncertainties associated with the heat flux measurements, it is difficult to illicit the truth using this method with high confidence using most of the sensors. With this method sensors one, two, five, six, and eight give more weight to hypothesis one. Sensors three, four, and seven are unable to determine the true origin scenario. A drawback to this approach is that it is difficult to quantify clearly by how much a hypothesis is more likely than the others.

**Table 4**
**Percentage of Heat Flux Measurements that Lie Within the Interval, $\bar{q}_{jn} - t^*\sigma \leq \hat{q}_{ijn} \leq \bar{q}_{jn} + t^*\sigma$, for Hypotheses One, Two, and Three**

| Sensor No. | Hypothesis 1 (%) | Hypothesis 2 (%) | Hypothesis 3 (%) |
|---|---|---|---|
| Sensor 1 | 100 | 93.9 | 76.0 |
| Sensor 2 | 100 | 97.4 | 95.3 |
| Sensor 3 | 100 | 100 | 100 |
| Sensor 4 | 100 | 99.9 | 100 |
| Sensor 5 | 99.7 | 97.8 | 89.2 |
| Sensor 6 | 100 | 99.7 | 99.7 |
| Sensor 7 | 100 | 100 | 98.8 |
| Sensor 8 | 100 | 99.9 | 99.2 |

## 5. Conclusions

The purpose of the analysis was to highlight the importance of sensor characteristics in the testing of fire evolution hypotheses using a well controlled experimental system. The study demonstrates the importance of quantifying the relevant uncertainties in measurements before going through an inference process. Critical to generating high quality data was an experimental compartment with multiple, electronically controlled burners and an array of well calibrated sensors. The experiments and analysis shown here are quite far removed from what a fire investigator in the field would be attempting to accomplish. In a real scenario the HRRs of the fires representing HRRs of possible objects in a compartment are unlikely to be all the same. Similarly ignition criteria and ventilation conditions will differ. The investigator, in a real scenario, will generally only have access to the post-fire compartment. The time integrated nature of the observed damage in the post-fire compartment will obfuscate temporal signatures of the fire-evolution.

With the simple experiments presented here, it was important to determine whether the true evolution scenario could be determined using a Bayesian framework exercised on temporal measurements. Even for a case where temporal data are available, some sensors might not be useful in distinguishing between hypotheses. Also, providing an improved error/uncertainty model for the sensors was critical to discriminating hypotheses when the sensor location was not properly chosen. In the future, more realistic experimental configurations are planned to address the issues of uncertainty in ventilation conditions, HRR, and damage signatures to sensor surrogates. The use of forward models capable of simulating the complex conditions in real fire compartments will also be explored as a tool for determining the true fire evolution from experimental measurements.

## Acknowledgements

This work is supported by U.S. National Science Foundation under Award No. 1707090.

## References


1. NFPA (2014) NFPA 921-guide for fire and explosion investigations. National Fire Protection Association
2. Strengthening forensic science in the united states: A path forward. Technical report, National Research Council (2009)
3. Gorbett GE, Chapdelaine W (2014) Scientific method-use, application, and gap analysis for origin determination. In: International symposium on fire investigation science and technology
4. Cox A (2013) Origin matrix analysis: a systematic methodology for the assessment and interpretation of compartment fire damage. Fire Arson Investig 64(1):1–27
5. Gorbett GE, Meacham BJ, Wood CB, Dembsey NA (2015) Use of damage in fire investigation: a review of fire patterns analysis, research and future direction. Fire Sci Rev 4:1–35. https://doi.org/10.1186/s40038-015-0008-4
6. Gorbett GE, Wood CB (2017) Structure and evaluation of the process for origin determination in compartment fires. Fire Technol 53:301–327
7. Hopkins RL, Gorbett G, Kennedy P (1997) Fire pattern persistence and predictability on interior finish and construction materials during pre and post flashover compartment fires. Technical report
8. Madrzykowski D, Fleischmann C (2012) Fire pattern repeatability: a study in uncertainty. J Test Evaluat 40(1):1
9. Madrzykowski D, Weinschenk C (2019) Impact of fixed ventilation on fire damage patterns in full-scale structures. Technical report, UL Firefighter Safety Research Institute
10. Stauffer E (2019) Interpol review of fire investigation 2016–2019. Forensic Science International, pp 1–14
11. Nordgaard A, Rasmusson B (2017) The likelihood ratio as value of evidence—more than a question of numbers. Fire Technol 53:301–327
12. Wang J, Zabaras N (2004) A Bayesian inference approach to the inverse heat conduction problem. Int J Heat Mass Transf 47:3927–3941
13. Biedermann A, Taroni F, Delemont O, Semadeni C, Davison AC (2005) The evaluation of evidence in the forensic investigation of fire incidents (part i): an approach using Bayesian networks. Forensic Sci Int 147(1):49–57
14. Biedermann A, Taroni F, Delemont O, Semadeni C, Davison AC (2005) The evaluation of evidence in the forensic investigation of fire incidents. Part II. Practical examples of the use of Bayesian networks. Forensic Sci Int 147(1):59–69
15. Overholt KJ, Ezekoye OA (2012) Characterizing heat release rates using an inverse fire modeling technique. Fire Technol 48:893–909
16. Overholt KJ (2013) Forward and inverse modeling of fire physics towards fire scene reconstructions. Ph.D. thesis, The University of Texas at Austin, Austin, TX
17. Overholt KJ, Ezekoye OA (2014) Quantitative testing of fire scenario hypotheses: a bayesian inference approach. Fire Technol 51(2):335–367
18. Kurzawski AJ, Cabrera JM, Ezekoye OA (2019) Model considerations for fire scene reconstruction using a bayesian framework. Fire Technol 56:1–23. https://doi.org/10.1007/s10694-019-00886-w
19. Weinschenk C, Beal CM, Ezekoye OA (2011) Modeling fan-driven flows for firefighting tactics using simple analytical models and CFD. J Fire Protect Eng 21:85–114
20. Overholt K, Ezekoye OA (2014) Quantitative testing of fire scenario hypotheses, a bayesian inference approach. Fire Technol 51:335–367

21. Kurzawski AJ (2017) Inverse modeling and characterization of an experimental testbed to advance fire scene reconstruction. Ph.D. thesis, The University of Texas at Austin, Austin, Texas
22. Standard methods of fire tests for evaluating contribution of wall and ceiling interior finish to room fire growth. Standard, National Fire Protection Agency (2019)
23. American Society for Testing and Materials, West Conshohocken, Pennsylvania. ASTM E 3057-16 Standard Test Method for Measuring Heat Flux Using Directional Flame Thermometers with Advanced Data Analysis Techniques (2016)
24. Cabrera JM, Moser RD, Ezekoye OA (2020) A modified directional flame thermometer: development, calibration, and uncertainty quantification. J Verif Valid Uncertain Quant 5:1–10
25. Rasmussen CE, Williams CKI (2006) Gaussian processes for machine learning. MIT Press, Cambridge